Monthly Notices
of the
ROYAL ASTRONOMICAL SOCIETY

MNRAS **481,** 3348–3356 (2018)
Advance Access publication 2018 September 10

doi:10.1093/mnras/sty2467

The evolution of Kerr discs and late-time tidal disruption event light curves

Steven A. Balbus ★ and Andrew Mummery ★
Oxford Astrophysics, Denys Wilkinson Building, Keble Road, Oxford, OX1 3RH, UK

Accepted 2018 September 6. Received 2018 September 5; in original form 2018 July 3

ABSTRACT

An encounter between a passing star and a massive black hole at the centre of a galaxy, a so-called tidal disruption event or TDE, may leave a debris disc that subsequently accretes on to the hole. We solve for the time evolution of such a TDE disc, using an evolutionary equation valid for both the Newtonian and Kerr regimes. The late-time luminosity emergent from such a disc is of interest as a model diagnostic, as it tends to follow a power law decline. The original simple ballistic fallback model, with equal mass in equal energy intervals, produces a $-5/3$ power law, while standard viscous disc descriptions yield a somewhat more shallow decline, with an index closer to -1.2. Of four recent, well-observed TDE candidates however, all had fall-off power-law indices smaller than one in magnitude. In this work, we revisit the problem of thin disc evolution, solving this reduced problem in full general relativity. Our solutions produce power-law indices that are in much better accord with observations. The late-time observational data from many TDEs are generally supportive, not only of disc accretion models, but of finite stress persisting down to the innermost stable circular orbit.

Key words: accretion, accretion discs – black hole physics – turbulence.

1 INTRODUCTION

The evolution of thin accretion discs is generally studied via techniques first developed by Lynden-Bell & Pringle (1974, hereafter LBP; Pringle 1981 for a review). They showed that an evolving thin Keplerian disc, subject to a viscous torque, obeyed a simple diffusion-like equation. The classical (Newtonian) disc evolutionary equation has found practical use in many astrophysical systems, including dwarf nova eruptions (Frank et al. 2002), protoplanetary discs (Fromang, Balbus, & Terquem 2002) and, the topic of this paper, tidal disruption events (hereafter TDEs) (Cannizzo, Lee & Goodman 1990). While *equilibrium* relativistic thin disc theory was developed nearly half a century ago, the ability to study relativistic disc evolution by the methods similar to those introduced by LBP is only now being developed. Riffert (2000) also examined the spreading of viscous discs in the relativistic regime, but for reasons that we will discuss in Section 2.4.2 below, out treatment differs somewhat from this. As an alternative to the much more expensive direct numerical simulation, the one-dimensional relativistic equation promises to be a practical theoretical tool, occupying the middle ground between computational rigour and phenomenological modelling.

In one of the appendices of a paper studying magnetic stresses in accretion discs, Eardley & Lightman (1975) first presented the form of this evolutionary appropriate for Kerr spacetime.[1] Following the Novikov & Thorne (1973) and Page & Thorne (1974) equilibrium models, the viscosity (in reality turbulent transport) is represented by an anomalous stress tensor. First invoked by Shakura & Sunyaev (1973), the anomalous stress both enhances the transport of angular momentum and drives significant dissipative heating. Emerging in the form of radiative losses, the latter energy source is the mechanism by which X-ray emitting accretion discs are ultimately observed.

Very little was done by way of investigating explicit solutions of the Eardley–Lightman equation until very recently, when Balbus (2017), unaware of the earlier derivation, rediscovered the Kerr evolutionary equation (in slightly different coordinates), and presented formal WKB modal solutions for both finite and vanishing stress inner disc bondary conditions. In this work, we examine solutions of the Kerr disc equation more generally, with a focus on the bolometric light curves, and compare their late-time evolution with TDEs (Rees 1988). Our goal is to understand some pertinent but puzzling features suggested by the observational data. A recent compilation by Auchettl, Guillochon, & Ramirez-Ruiz (2017; hereafter AGR) is revealing. At late times, TDEs are expected to display light curves $L(t)$ that vary as a power law n in time t, $L \sim t^n$. The original Rees

★ E-mail: Steven.Balbus@astro.ox.ac.uk (SAB);
andrew.mummery@wadham.ox.ac.uk (AM)

[1] We are grateful to P. Ivanov for drawing this paper to our attention.

© 2018 The Author(s)
Published by Oxford University Press on behalf of the Royal Astronomical Society

Downloaded from https://academic.oup.com/mnras/article-abstract/481/3/3348/5094593 by Said Business School user on 14 November 2018

(1988) 'fallback' model, which assumed equal mass in equal energy intervals (and ballistic dynamics), leads to $n = -5/3$. Disc accretion models (Cannizzo et al. 1990) extend the duration of the emission somewhat, with a typical index of $n \simeq -1.2$. However, the late-time AGR power-law indices of confirmed X-ray TDEs clustered around $n \simeq -0.75$, a much more shallow fall-off. There is no widely accepted explanation of how such an X-ray index might arise. We put forth here a simple and rather surprising solution to this puzzle: something very close to this value is expected from a population of time-dependent accreting Keplerian discs. The difference between our findings and those of Cannizzo et al. (1990) arises from our technique of smoothly joining an outer Keplerian disc solution to an inner relativistic disc, which then terminates at an innermost stable circular orbit (ISCO), which may have finite stress. The presence of this ISCO boundary zone is itself hardly involved with the *direct* production of the light curve – it is the external Keplerian zone that is responsible for the bulk of the observed luminosity. Nevertheless, the ISCO boundary condition is important because it results in a slightly different admixture of external Keplerian modes (exponentially declining Laplace transforms) compared with the pure Newtonian disc. The altered admixture in turn alters the late-time dependence of the disc's thermal emission, ultimately leading to a less-steep decline, a sort of feedback effect. Encouragingly, this also is what observations seem to show.

Note that the solutions we describe here in principle allow for a measurement of the stress present at the ISCO: the outer Keplerian combination of modes, and thus the late-time luminosity, depend rather sensitively on whether the stress vanishes at the ISCO radius or not. We find that the imposition of a vanishing stress tensor leads to a much steeper fall-off in $L(t)$, one that replicates the late-time behaviour seen in the Cannizzo et al. (1990) calculations. This, however, accords less well with observations. A non-vanishing stress condition at the ISCO, by contrast, tips the outer modal balance and leads to a more shallow fall-off for $L(t)$, in better accord with the data. This interesting point and how it relates to the stability arguments in Balbus (2017) (which advanced a vanishing stress condition!) is discussed more fully in Section 3. The question of finite versus vanishing stress at the ISCO still remains a point of contention within the disc community.

The plan of this paper is as follows. In Section 2, we lay out the fundamental solution to the Kerr evolutionary equation. We first present the results of direct numerical integration, both for the case of finite stress at the ISCO as well as for vanishing stress. The late-time luminosity behaviour is found to be well fit by a declining power law in both cases, but with a much steeper fall-off for the vanishing ISCO stress. The finite stress case appears to be compatible with observed results of confirmed TDEs. The numerical integration is followed by an analysis of Laplacian-Bessel normal modes of the disc system. With the appropriate ISCO boundary conditions, it is possible to understand why the two different late-time behaviours arise. Finally in Section 3 we discuss the observational implications of our findings, note the limitations of our simple model, and suggest further developments motivated by the present encouraging study. The Appendices contain technical mathematical details pertinent both to the numerical and analytic discussions.

We observe the same notational conventions of Balbus (2017). The speed of light is set to unity throughout. Greek indices $\alpha, \beta, \gamma \ldots$ generally denote spacetime coordinates. The exception is ϕ, which is reserved exclusively for the azimuthal angular coordinate. The time coordinate is labelled 0. The metric in local inertial coordinates is $g_{\alpha\beta} \rightarrow \eta_{\alpha\beta} = \mathrm{diag}(-1, 1, 1, 1)$. Other notation is standard: G is the gravitational constant, M the central black hole mass, J the central black hole angular momentum, $a = J/M$ the black hole spin parameter, and $r_g = GM$ the gravitational radius.

2 ANALYSIS

2.1 Governing equation

Our coordinates are cylindrical Boyer–Lindquist for a Kerr disc: r (radial), ϕ (azimuthal), and z (vertical). We seek the evolution of the azimuthally averaged, height-integrated disc surface density $\Sigma(r, t)$. The contravariant four velocity of the disc fluid is U^μ; the covariant counterpart is U_μ. The specific angular momentum corresponds to U_ϕ, a covariant quantity. There is an anomalous stress tensor present, $W^r{}_\phi$, due to low-level disc turbulence, which is a measure of the correlation between the fluctuations in U^r and U_ϕ (Eardley & Lightman 1975; Balbus 2017). This is, as the notation suggests, a mixed tensor. As noted earlier in the Introduction, $W^r{}_\phi$ serves both to transport angular momentum as well as to extract the free-energy of the disc shear, which is then thermalized and radiated from the disc surface, both assumed to be local processes.

We will work with the quantity

$$Y \equiv \sqrt{g}\,\Sigma\, W^r{}_\phi, \tag{1}$$

where $g > 0$ is the absolute value of the determinant of the (midplane) Kerr metric tensor $g_{\mu\nu}$. The governing equation for the evolution of the disc is then given by (Balbus 2017):

$$\frac{\partial Y}{\partial t} = \frac{W^r{}_\phi}{U^0}\frac{\partial}{\partial r}\frac{1}{U'_\phi}\left[\frac{\partial Y}{\partial r} - U_\phi U^\phi (\ln\Omega)' Y\right], \tag{2}$$

where the primed notation $'$ denotes an ordinary derivative with respect to r. A direct rendering, or 'relativistic upgrade,' from the original Newtonian equation (Pringle 1981; Balbus & Papaloizou 1999), would end with the first term on the right. The second term is a further relativistic correction stemming from the photon angular momentum loss. Note that if $W^r{}_\phi$ has a functional dependence on Σ, the stress would be implicitly time dependent. In that case, equation (2) should be modified to:

$$\frac{\partial (Y/W^r{}_\phi)}{\partial t} = \frac{1}{U^0}\frac{\partial}{\partial r}\frac{1}{U'_\phi}\left[\frac{\partial Y}{\partial r} - U_\phi U^\phi (\ln\Omega)' Y\right]. \tag{3}$$

The metric tensor has disappeared from the evolutionary equation in any explicit form, entering implicitly from the definition of Y.

Before proceeding to solutions of equation (2), let us recall its limitations. We are of course using thin disc theory, which ignores terms of quadratic or higher order in the ratio of the disc scale height to radius, H/r. This is equivalent to ignoring pressure terms relative to those involving rotational energy. Abramowicz et al. (1988) investigated the effects of such terms on the accretion of 'slim discs' (which assumes small but finite H/r), noting their importance near the ISCO. Here it should be noted that the validity of equation (2) does not depend on the neglect of pressure relative to rotation; it depends only on the notion that the concept of some sort of suitably averaged $W^r{}_\phi$ turbulent tensor makes sense. In this respect, it is no more restrictive than any reduced theory of disc turbulence, which in essence includes all theoretical modelling of such flow. Where thin disc theory may be inaccurate is in its handling of the energetics, for which it assumes efficient local radiation. This is indeed likely to break down near the ISCO. As we will see, however, the net luminosity emerging from our solutions appears to be dominated by the inner, but still robustly Keplerian, regions of the disc. It is therefore useful to develop and understand the predictions of thin

Downloaded from https://academic.oup.com/mnras/article-abstract/481/3/3348/5094593 by Said Business School user on 14 November 2018

disc theory, while granting its omissions and shortcomings, which invite further consideration.

2.2 Compact formulation and a simple analogue model

In this paper, we will work entirely with equation (2). Following Balbus (2017), we define Q by

$$\frac{\mathrm{d}Q}{\mathrm{d}r} = -U_\phi U^\phi (\ln \Omega)'. \tag{4}$$

Equation (A19) in Appendix A1 shows that for Kerr geometry, we have the useful identity

$$e^{-Q} = U^0. \tag{5}$$

Then, with

$$\zeta = Y/U^0, \tag{6}$$

equation (2) becomes

$$\frac{\partial \zeta}{\partial t} = \frac{W^r{}_\phi}{(U^0)^2}\frac{\partial}{\partial r}\frac{U^0}{U'_\phi}\left[\frac{\partial \zeta}{\partial r}\right]. \tag{7}$$

While the full dynamical equation (2) may be solved directly by numerical methods (we do so in Section 2.3 below), it is helpful to have a simplified 'toy model' that retains essential features of the full problem in a mathematically accessible form that may be addressed analytically. The function U^0 reduces to unity in the Newtonian limit, and over the entire domain of interest in Kerr geometry, it is smooth, non-vanishing, and bounded. The qualitative content of equation (7) may thus be retained by ignoring these functions, in effect setting them equal to unity. By contrast, U'_ϕ vanishes at the ISCO, introducing an apparent singularity into the equation, and must be handled with more care. We will restrict ourselves to the relatively simple case of Schwarzschild geometry for analytic treatment, as this illustrates many of the salient features of the full Kerr problem in a more tractable setting. Our model equation thus takes the form:

$$\frac{\partial y}{\partial t} = W^r{}_\phi \frac{\partial}{\partial r}\left[\frac{1}{U'_\phi}\frac{\partial y}{\partial r}\right]. \tag{8}$$

We use the lowercase y to distinguish our model from the true surface density variable Y.

2.3 Numerical formulation and solution

We begin with a summary of the exact numerical solution of equation (7). The interested reader will find technical details discussed in Appendix A1. Some care is needed in handling the numerically singular behaviour near the ISCO, where U'_ϕ vanishes.

The mathematical problem to be solved is the evolution of a very compact Gaussian ring, in effect of the Green's function solution. The ring is initially located at $r_0 = 15.75\, r_g$, a fiducial tidal radius taken from Rees (1988), ∼2.6 times the ISCO radius of a Schwarzschild hole (see below). At this location, relativity is by no means negligible. While the short-term evolution depends on the initial radius chosen, the long-term evolution of the extended disc does not.

2.3.1 ISCO boundary conditions

A representative case is shown in Fig. 1. At early times, the disc spreads both radially inwards and outwards. As the inner edge

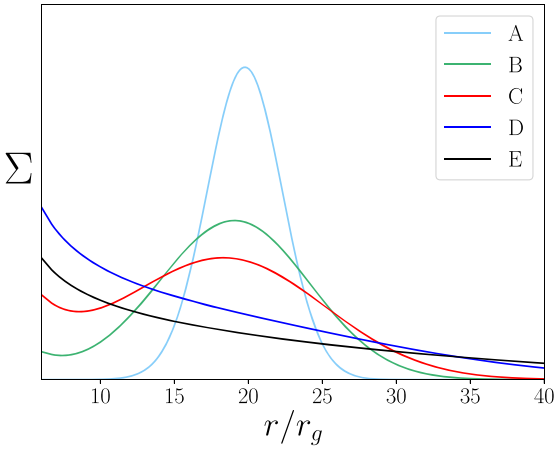

Figure 1. Evolution of the surface density in the Schwarszchild metric. The lines A–E are at progressively later times, showing the initial inwards drift of debris before the ISCO surface density decreases with time. The dimensionless time values (equation A9) for the different stages of evolution are: $\tau = 0.06$(A), 0.24(B), 0.43(C), 1.84(D), and 6.06(E).

reaches the ISCO, a boundary condition must be specified, the precise nature of which depends on the behaviour of the turbulent stress at the ISCO. If vanishing stress is imposed, the surface density and thus the local emissivity must also vanish. For finite ISCO stress, we show in Appendix A1 that the proper boundary condition is that the radial gradient of ζ must vanish, as opposed to ζ itself. Numerically, the value of ζ at the innermost (ISCO) grid point is set equal to its value at the adjacent external grid point.

2.3.2 Kerr disc, finite ISCO stress, $W^r_\phi \propto r^{-1/2}$

Using equation (A31) from Appendix A1, we have evaluated the luminosity profiles $L(t)$ for discs evolving in the Kerr geometry. for a variety of different black hole spins a. As noted, each disc had the same mass and was initially laid down at $r = 15.75 r_g$, the tidal radius for a solar mass star orbiting a $10^6 M_\odot$ black hole (Rees 1988). $W^r_\phi \propto r^{-1/2}$ corresponds to a constant viscosity model, chosen merely as benchmark. Once the stress at the ISCO is specified, our results are not very sensitive to the precise parametrization of W^r_ϕ. But the late-time behaviour does depend sensitively on whether this stress is finite or vanishing.

Even within the restrictions of this simple model, observational TDE emission profile features emerge: a rapid increase in intensity followed by a gradual monotonic power law decrease in intensity at late times. The luminosity $L(t) \sim t^n$, with n typically between -0.6 and -0.7. Typical fits are shown by the solid lines in Fig. 2. The best-fitting values of the decay index, n, are shown in Table 1 for several black hole angular momenta. These solutions are in better accord with late-time observations of confirmed TDEs than the classical Newtonian discs with vanishing inner stress. In particular, the finite stress power-law index is always less steep than t^{-1}, whereas the Newtonian discs are generally steeper than t^{-1} (Cannizzo et al. 1990). This is a potentially important result which is developed below.

2.3.3 Kerr disc, finite ISCO stress, $W^r_\phi \propto r^\mu$

The general agreement between our numerical solutions and the observational decay indices for the case of finite ISCO stress is not

Downloaded from https://academic.oup.com/mnras/article-abstract/481/3/3348/5094593 by Said Business School user on 14 November 2018

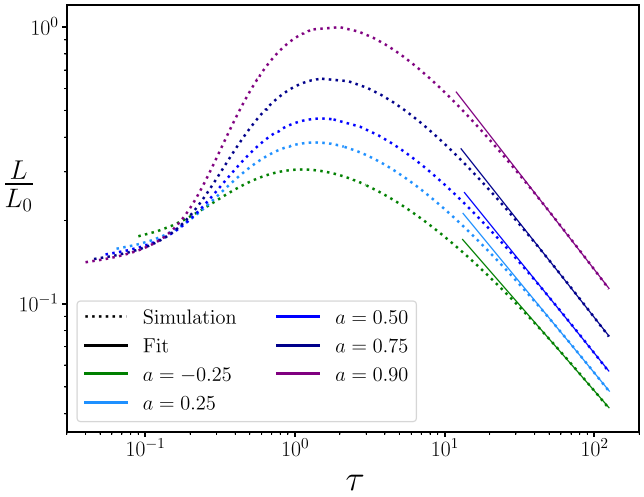

Figure 2. Luminosity profiles for a selection of different black hole angular momenta. L_0 is the $a/r_g = 0.9$ peak luminosity. The dimensionless time τ as defined in equation (A9) is plotted on the x-axis. Each profile is well fit by a (straight line) power law at late times. See Table 1 for power-law values.

Table 1. Best-fitting late-time luminosity decay indices, in the case of finite ISCO stress, for different black hole spin.

a/r_g	n
−0.5	−0.6
−0.25	−0.62
0	−0.65
0.25	−0.66
0.5	−0.67
0.75	−0.69
0.9	−0.7

Table 2. Comparison between late-time numerically determined luminosity decay indices and the analytical form equation (A11). W^r_ϕ is assumed to vary as r^μ (therefore finite at the ISCO), and $a/r_g = 0.9$ here, rapid rotation.

Stress Index μ	n (numerical)	n (equation A11)
1/2	−0.45	−0.5
0	−0.61	−0.67
−1/2	−0.70	−0.75
−1	−0.76	−0.8
−3/2	−0.78	−0.83
−2	−0.80	−0.86

a special feature of a particular r-dependence of the turbulent stress. Table 2 shows the best-fitting decay indices for a rapidly rotating black hole, $a/r_g = 0.9$, for a number of different turbulent stress profiles, parametrized as a power law by μ, $W^r_\phi \propto r^\mu$. The analytic value of n from equation (A11) is appropriate to a Green's function superposition of negative index Bessel functions (See Appendix for further details). The true solution is somewhat more complicated, and thus only rough agreement is expected. These results nevertheless serve to demonstrate that the exact radial dependence of the turbulent stress is hardly crucial for general agreement between numerical and observational results. This robustness is important,

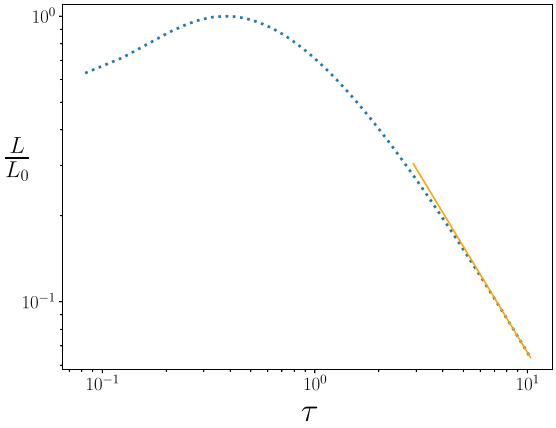

Figure 3. The Luminosity $L(t)$ for the case of vanishing stress at the ISCO, based on solving the full Kerr equation (7). The fitted late-time behaviour $L \sim t^{-1.23}$, agrees very closely with the Newtonian solution, $L \sim t^{-5/4}$. The dimensionless time τ as defined in equation (A9) is plotted on the x-axis.

Table 3. The four well-observed sources from AGR (left) and their deduced late-time luminosity power-law index (right).

ASASSN-14li	−1.0
Swift J1644+57	−0.71
Swift J2058+05	−0.16
XMMSL1 J0740-85	−0.75

as the particular form of the turbulent stress is not known in detail, apart from an expectation that the stress is likely to fall-off gradually with distance.

2.3.4 *Kerr disc, vanishing ISCO stress*

For this numerical model, the stress vanished near the ISCO (r_I) as $W^r_\phi \propto (r - r_I)^2$ near the ISCO (Balbus 2017). This behaviour continues through $r = 10r_g$, at which point it switches piecewise continuously to $W^r_\phi \propto r^{-1/2}$ for $r > 10r_g$. The luminosity profile $L(t)$ for a Schwarzschild black hole ($r_I = 6r_g$, $a = 0$) is displayed in Fig. 3.

The best-fitting decay index for vanishing ISCO stress, $n = -1.23$, is sharply different from all of the non-vanishing stress cases, but very similar to the Cannizzo et al. (1990) canonical Newtonian value of $-19/16 \simeq -1.19$. The steeper fall-off is sharply discrepant with the observations showing a distinctly more shallow fall-off with time (Table 3). This suggests that in determining the late-time luminosity behaviour both the stress boundary condition and relativistic dynamics are of importance, neither can alone reproduce the observational results.

2.3.5 *Summary of numerical results*

We have numerically integrated the time-dependent solutions of equation (7), the thin disc equation for the evolution of a turbulent disc. Two different inner boundary conditions were explored, that of vanishing stress at the ISCO and finite stress. For the former, ζ vanishes at the ISCO, while for the latter, the radial gradient of ζ vanishes. This produces two very distinct late-time behaviours for the integrated luminoisty $L(t)$, with the finite stress solutions falling of less rapidly than t^{-1} and the vanishing stress solutions

Downloaded from https://academic.oup.com/mnras/article-abstract/481/3/3348/5094593 by Said Business School user on 14 November 2018

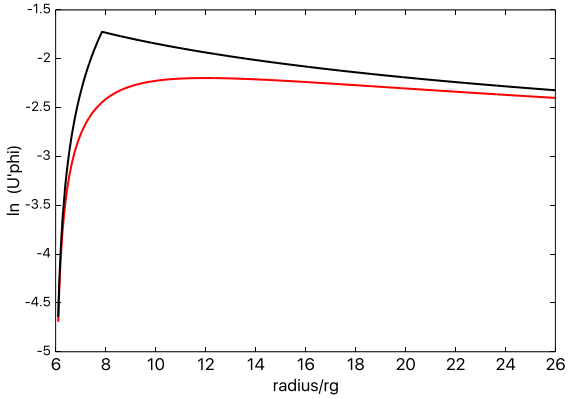

Figure 4. $\ln U'_\phi$ versus r/r_g. Piecewise continuous fit (in black) to exact Schwarzschild equation (10) (in red), based on the ISCO approximation (11) for $r \le r_m$, and the Keplerian form (12) for $r \ge r_m$. U'_ϕ calculated with $r_g = 1$.

more rapidly than t^{-1}. The latter are in good accord with earlier Newtonian disc calculations, but the former are in better accord with observations. The dichotomy of luminosity falling more steeply than t^{-1} for vanishing ISCO stress and less rapidly than t^{-1} for finite ISCO stress persists with different hole angular momenta, and is insensitive to stress behaviour non-local to the ISCO.

It has been argued that vanishing stress at the ISCO may be expected on the grounds of stability (Balbus 2017), but clearly this question needs to be revisited!

2.4 Analytic modal solutions of the reduced equation

We may understand the key features of our numerical solutions, such as the dichotomy of $L(t)$ power-law fall-offs, by examining the Laplace modes of a reduced disc model. This involves adopting a simple piecewise continuous form for U'_ϕ.

2.4.1 *Piecewise continuous form for* U'_ϕ

The Schwarzschild metric angular frequency Ω is given by

$$\Omega = \frac{\mathrm{d}\phi}{\mathrm{d}t} = \frac{U^\phi}{U^0} = \sqrt{\frac{r_g}{r^3}}, \tag{9}$$

and the angular momentum gradient is

$$U'_\phi = \frac{\Omega}{2}\frac{r-6r_g}{(1-3r_g/r)^{3/2}} = \frac{\sqrt{r_g}}{2}\frac{r-6r_g}{(r-3r_g)^{3/2}}. \tag{10}$$

The angular momentum gradient U'_ϕ vanishes at the ISCO radius $r_I = 6r_g$ and approaches $r\Omega/2$ in the Keplerian zone, $r \gg r_g$. For analytic purposes, we will model U'_ϕ near the ISCO by its local linear form

$$U'_\phi = \sqrt{2}\Omega_I(r-r_I) \equiv \sqrt{2}\Omega_I x \quad \text{(ISCO)}, \tag{11}$$

where $\Omega_I = \sqrt{r_g/r_I^3}$ and $x = r - r_I$. In the outer Keplerian disc, we have as usual

$$U'_\phi = \frac{r\Omega}{2} = \frac{1}{2}\sqrt{\frac{GM}{r}} \quad \text{(Kepler)}. \tag{12}$$

Our model angular momentum gradient, denoted u'_ϕ, will be the piecewise continuous compilation of equations (11) and (12), as shown in Fig. 4. Extrapolating equation (11) to the point where it matches equation (12) at the radius denoted r_m, we have

$$u'_\phi = \sqrt{2}\Omega_I(r-r_I) \quad (r < r_m)$$
$$u'_\phi = \frac{r\Omega}{2} \quad (r \ge r_m). \tag{13}$$

The matching radius r_m is determined by continuity of u'_ϕ at $r = r_m$, the radius at which the two curves cross:

$$r_m/r_g = 3(3+\sqrt{5})/2 = 7.854, \tag{14}$$

which is slightly beyond the ISCO radius $6r_g$. This gives

$$x_m/r_g = 3(\sqrt{5}-1)/2 = 1.854.$$

Here, for the sake of simplicity, we will assume constant W^r_ϕ, denoted in the model as w (With dimensions of length $\times$ velocity^2, a self-similar Keplerian stress tensor W^r_ϕ would in fact lead to a constant-with-r scaling). This obviously implies a *non-vanishing* ISCO stress; we consider the case of vanishing ISCO stress in Section 2.6.2. Our formal reduced equation takes the form

$$\frac{\partial y}{\partial t} = w\frac{\partial}{\partial r}\left[\frac{1}{u'_\phi}\frac{\partial y}{\partial r}\right]. \tag{15}$$

For $r < r_m$ this becomes:

$$\frac{\partial y}{\partial t} = \frac{w}{\sqrt{2}\Omega_I}\frac{\partial}{\partial x}\left[\frac{1}{x}\frac{\partial y}{\partial x}\right], \tag{16}$$

while for $r \ge r_m$ the equation is

$$\frac{\partial y}{\partial t} = \frac{2w}{\sqrt{GM}}\frac{\partial}{\partial r}\left[r^{1/2}\frac{\partial y}{\partial r}\right]. \tag{17}$$

The joining boundary condition is continuity of y and dy/dr at $r = r_m$.

2.4.2 *Laplace modes*

We seek stable solutions with time dependence e^{-st}, $s \ge 0$, i.e. Laplace transforms. The solution for a particular initial condition is then a superposition of such (mathematically complete) modes. The reduced ISCO equation (16) now reads

$$-\frac{s\sqrt{2}\Omega_I}{w}y = \frac{\mathrm{d}}{\mathrm{d}x}\left[\frac{1}{x}\frac{\mathrm{d}y}{\mathrm{d}x}\right]. \tag{18}$$

The desired stable mode that decays exponentially inside the ISCO ($x < 0$) and is oscillatory for $x > 0$ is:

$$y = \mathrm{Ai}'(-kx), \qquad k^3 = \frac{s\sqrt{2}\Omega_I}{w}, \tag{19}$$

as noted in Balbus (2017) for this same problem. Here Ai is the usual Airy function (Abramowicz & Stegun 1965) and Ai$'$ is the derivative with respect to its argument. This solution is valid for $r_I \le r \le r_m$, and in effect constitutes the appropriate finite stress inner boundary condition: the exterior, Newtonian domain solution must join smoothly on to the inner soultion (equation 19). Note that this condition is different to that of Riffert (2000), who set the density at the ISCO to zero by way of imposing a vanishing stress boundary condition.

For $r \ge r_m$, the Keplerian form (equation 17) is appropriate. Writing this in terms of $\xi = \sqrt{r}$ leads to:

$$-\frac{s\sqrt{GM}}{2w}\xi y = \frac{\mathrm{d}^2 y}{\mathrm{d}\xi^2}, \qquad \xi \equiv r^{1/2}. \tag{20}$$

Downloaded from https://academic.oup.com/mnras/article-abstract/481/3/3348/5094593 by Said Business School user on 14 November 2018

This equation has two linearly independent solutions, y_+ and y_-, where

$$y_\pm = \sqrt{\xi} J_{\pm 1/3}\left(\frac{2\alpha}{3}\xi^{3/2}\right), \quad \alpha^2 = \frac{s\sqrt{GM}}{2w}, \tag{21}$$

where $J_{1/3}$ and $J_{-1/3}$ are standard Bessel functions of order 1/3 and $-1/3$, respectively. In general, the outer Kelplerian zone solution will take the form of a linear superposition

$$y = C_1 y_- + C_2 y_+, \tag{22}$$

where C_1 and C_2 are constants determined by joining this outer Keplerian solution and its first derivative smoothly to the inner solution (equation 19) at the matching radius r_m. In general, these two constraints can be satisfied only by a superposition of both y_+ and y_-, and it is this admixture that determines the late-time behaviour of the general solution.

2.5 Newtonian versus Kerr discs

In a strictly Newtonian system, equation (17) has only one solution that leaves Σ finite as $r \to 0$, the solution y_+

$$y_+ = \sqrt{\xi} J_{1/3}\left(\frac{2\alpha}{3}\xi^{3/2}\right), \tag{23}$$

which vanishes linearly in r in this limit. The superposition integral (Gradshteyn & Ryzhik 2014)

$$\int_0^\infty J_p(\sqrt{s}X) J_p(\sqrt{s}X_0) e^{-st}\,\mathrm{d}s = \frac{1}{t}\exp\left(\frac{-X^2 - X_0^2}{4t}\right) I_p\left(\frac{XX_0}{2t}\right), \tag{24}$$

tells us how to construct the Green's function for J_p modes. Here p is any complex number whose real part exceeds -1, and I_p is the standard modified Bessel function. The right side is proportional to a delta function $\delta(X - X_0)$ as $t \to 0$, a result that is independent of p. Note that while we can always multiply y_+ by an arbitrary function of s and retain a true mode, the particular Green's function superposition (equation 24) requires a Bessel function of the form shown in equation (23) with no s-dependent coefficient.

The late time $t \to \infty$ asymptotic behaviour of the I_p function leads to a time dependence in the surface density scaling as

$$\Sigma \sim \frac{1}{t^{1+p}}. \tag{25}$$

As this is the only quantity that varies with time in the emission integral, this is also the late-time power-law time dependence of the total luminosity L. This leads to a $t^{-4/3}$ dependence in our simple constant angular momentum stress model ($p = 1/3$), but it is not very sensitive to how the stress is modelled. A constant viscosity model leads to $t^{-5/4}$ (Pringle 1981), while a more complicated α-model produces values near $-19/16 \simeq -1.19$ (Cannizzo et al. 1990). Neither of these can be comfortably stretched to the observed peak near -0.75 in the late-time histogram of values given by Auchettl et al. (2017).

An initial $t = 0$ delta function superposition of $J_{-1/3}$ Bessel functions, on the other hand, would produce a late-time luminosity scaling $t^{-2/3}$, much closer to the observed AGR histogram peak. (A constant viscosity model at $t^{-3/4}$ is yet better.) The apparent difficulty is that these modes lead to singular behaviour in the surface density (and perhaps the mass accretion rate) as $r \to 0$.

In reality, the inner disc of a Kerr black hole is cut-off at the ISCO. The $r = 0$ singularity is not relevant to this type of calculation. Even in Newtonian modelling some inner disc cut-off is required to avoid a singularity in the accreted matter. But if $r = 0$ is actually outside the domain, we should expect a superposition of $J_{1/3}$ and $J_{-1/3}$ solutions to be present in the bulk of the disc. This in itself is not enough to guarantee late time $t^{-2/3}$ luminosity behaviour; it depends on the precise s-dependence of our modal superposition. But we now understand how in principle the more shallow late-time fall-off that emerges from direct numerical integration of equation (7) arises.

2.6 Construction of solution

2.6.1 *Finite ISCO stress*

We return now to the task of finding the matching coefficients C_1 and C_2 of the outer Keplerian zone solution by requiring continuity of y and its first derivative $\mathrm{d}y/\mathrm{d}r$ at the matching radius r_m. For future reference we note

$$\frac{\mathrm{dAi}'(-kx)}{\mathrm{d}r} = \frac{\mathrm{dAi}'(-kx)}{\mathrm{d}x} = -k\mathrm{Ai}'(-kx) = k^2 x\,\mathrm{Ai}(-kx), \tag{26}$$

where the prime $'$ denotes differentiation with respect to the displayed functional argument and the differential equation for the Airy function has been used in the final equality. Also, with y given by equations (21) and (22), standard Bessel function identities allow us to write

$$\frac{\mathrm{d}y}{\mathrm{d}r} = \frac{\alpha}{2}\left[-C_1 J_{2/3}\left(\frac{2\alpha}{3}r^{3/4}\right) + C_2 J_{-2/3}\left(\frac{2\alpha}{3}r^{3/4}\right)\right]. \tag{27}$$

To avoid a cluttered appearance in the equations, let us define

$$\tilde{\alpha} = 2r_m^{3/4}\alpha/3. \tag{28}$$

The matching conditions for y and $\mathrm{d}y/\mathrm{d}r$ at $r = r_m$ are then

$$\frac{\mathrm{Ai}'(-kx_m)}{r_m^{3/4}} = C_1 J_{-1/3}(\tilde{\alpha}) + C_2 J_{1/3}(\tilde{\alpha}) \tag{29}$$

$$\frac{2k^2 x_m}{\alpha}\mathrm{Ai}(-kx_m) = -C_1 J_{2/3}(\tilde{\alpha}) + C_2 J_{-2/3}(\tilde{\alpha}). \tag{30}$$

Solving for C_1 and C_2:

$$C_1 = \frac{\mathrm{Ai}'(-kx_m)\,J_{-2/3}(\tilde{\alpha})}{r_m^{3/4}\,\mathrm{Wr}} - \frac{2x_m k^2 \mathrm{Ai}(-kx_m)\,J_{1/3}(\tilde{\alpha})}{\alpha\,\mathrm{Wr}} \tag{31}$$

$$C_2 = \frac{\mathrm{Ai}'(-kx_m)\,J_{2/3}(\tilde{\alpha})}{r_m^{3/4}\mathrm{Wr}} + \frac{2x_m k^2 \mathrm{Ai}(-kx_m)\,J_{-1/3}(\tilde{\alpha})}{\alpha\mathrm{Wr}}, \tag{32}$$

where Wr is the Wronskian (Abramowitz & Stegun 1965):

$$\mathrm{Wr} \equiv J_{1/3}(\tilde{\alpha})J_{2/3}(\tilde{\alpha}) + J_{-1/3}(\tilde{\alpha})J_{-2/3}(\tilde{\alpha}) = \frac{3\sqrt{3}}{2\pi\alpha r_m^{3/4}}. \tag{33}$$

The late-time ($t \to \infty$) superposition of e^{-st} modes will be dominated by contributions from small s. In this limit, it is the $\mathrm{Ai}'J_{-2/3}$ term in the C_1 numerator that is dominant ($\sim s^{-1/3}$), and therefore so is C_1 itself. When the inner ISCO boundary hosts a non-vanishing stress, the late-time behaviour of the matching outer Keplerian zone is therefore dominated by the $J_{-1/3}$ modes. This is precisely what we would expect given a late-time power law of $-2/3$ for the luminosity and the (equation 24) superposition integral with $p = -1/3$.

2.6.2 *Vanishing ISCO stress*

If the stress tensor vanishes at the ISCO, then the local solution near $x = 0$ is (Balbus 2017):

$$y = xJ_2(2\sqrt{\beta x}), \quad \beta = 2s\sqrt{2}\Omega_I/W^r_\phi, \tag{34}$$

Downloaded from https://academic.oup.com/mnras/article-abstract/481/3/3348/5094593 by Said Business School user on 14 November 2018

where J_2 is the Bessel function of order two. Using (Abramowitz & Stegun 1965):

$$\frac{\mathrm{d}y}{\mathrm{d}r} = \sqrt{\beta x}\, J_1(2\sqrt{\beta x}). \tag{35}$$

The system of equations to be solved now is (suppressing the Bessel function arguments on the right side of the equations):

$$\frac{x_m J_2(2\sqrt{\beta x_m})}{r_m^{3/4}} = C_1 J_{-1/3} + C_2 J_{1/3} \tag{36}$$

$$\frac{2\sqrt{\beta x_m}\, J_1(2\sqrt{\beta x_m})}{\alpha} = -C_1 J_{2/3} + C_2 J_{-2/3}. \tag{37}$$

This is identical to the system (29) and (30) with $x_m J_2$ replacing Ai$'$ and $\sqrt{\beta x_m}\, J_1$ replacing $k^2 x_m$Ai. When not shown, the argument of all integer Bessel functions is understood to be $2\sqrt{\beta x_m}$; as before, fractional Bessel functions all have argument $2r_m^{3/4}\alpha/3$. The solution of this system is

$$C_1 = \frac{x_m J_2\ J_{-2/3}}{\mathrm{Wr}\ r_m^{3/4}} - \frac{2\sqrt{\beta x_m} J_1\ J_{1/3}}{\mathrm{Wr}\ \alpha} \tag{38}$$

$$C_2 = \frac{1}{\mathrm{Wr}}\left[\frac{x_m J_2\ J_{2/3}}{r_m^{3/4}} + \frac{2\sqrt{\beta x_m} J_1\ J_{-1/3}}{\alpha}\right]. \tag{39}$$

The small s scalings are

$$\alpha \sim s^{1/2}, \quad \beta \sim s, \quad J_p \sim s^{p/2} \quad \text{(for all } p\text{)}. \tag{40}$$

Now the dominant term for small s is the $J_1 J_{-1/3}$ group in the C_2 coefficient. This in turn means that the dominant contributing modes in the Keplerian zone are *positive* indexed, $J_{1/3}$ modes. Once again, this is just what is expected on the basis of a (24) modal superposition integral with $p = 1/3$ and from the observed late-time $t^{-4/3}$ time dependence found in the numerical simulations.

3 DISCUSSION

Figure 15 of AGR shows a histogram of power-law indices of X-ray selected TDEs. The curves have been separated by early (solid lines) and late-time (dashed lines) divisions, as well as whether the event is a strong TDE candidate (shown in blue) or only 'likely.' The dominant peak in the histogram is for late-time, likely X-ray TDEs, and it occurs for a power-law index of $n \simeq -0.75$. In fact, the histogram is somewhat schematic because there are only four well-observed late-time confirmed TDEs in the AGR sample. These, together with their inferred power-law index, are listed in Table 3. While errors in these values are somewhat difficult to assess, one significant figure is probably a reasonable working assumption, and what is therefore striking from this table is that none of these indices is larger than one (in magnitude). This accords nicely with our own numerical findings that Keplerian discs joining on to an inner, finite stress, ISCO region also do not have late-time power-law fall-offs in luminosity steeper than one. While it is premature to conclude that all late-time TDEs have settled into an accreting thin disc (there are too many ways for a 'train wreck' to unfold), there seems to be a case that at least some of them may well be. It is striking and gratifying that the classical Newtonian results may be recovered and that new solutions can be achieved from our approach, and that the latter offer a new theoretical route to understanding the shallow power-law luminosity fall-offs with completely conventional disc physics. We also remark in passing that, compared with direct interpretation of disc spectra, the late-time temporal behaviour of an evolving disc is a more powerful, less ambiguous, discriminator for the presence or absence of finite stress at the ISCO. The disadvantage is of course that the best time for observing this is when the source is faintest.

As we have noted, the question of whether the turbulent stress must vanish at the ISCO has been controversial; the view that it must vanish on dynamical grounds has retained prominent advocates (Paczyński 2000). Moreover, one of the current authors argued in an earlier paper (Balbus 2017) that a vanishing ISCO stress was to be expected on the grounds of greater stability. But simulations often show magnetic stress remaining finitely down to the ISCO (Noble, Krolik, & Hawley 2010), and there is a physical basis for understanding why an outward angular momentum flux constant should be present when the disc flow sharply transitions from rotational dominance to inward streaming (Agol & Krolik 2000). That a finite ISCO stress may in fact exhibit some degree of flow instability from the tunnelling of unstable modes from within the ISCO radius need not be a basis for rejection: this sort of behaviour in the region outside the ISCO is liable to be little more than orbital inspiral before turning to true plunging, once the ISCO is crossed. Indeed, something very much like this behaviour is observed in detailed numerical magnetohydrodynamic (MHD) simulations. The fundamental content of our analysis is likely to be preserved even with inspiraling near the ISCO, a claim that may now be checked by combining our semi-analytic approach with controlled 3D MHD simulations. In short, there seems to be nothing particularly unphysical about finite magnetic ISCO stresses. TDE light curves may well be a powerful observational constraint, if they consistently show late-time power-law indices less than unity.

Finally, we reiterate that discs are much more complicated than our 1970's era thin disc model. Real discs need not be thin; they have outflows, jets, coronae, and as yet poorly understood major state transitions. The main point, however, is that four decades after its inception, even the ordinary thin disc model has not been understood in all of its temporal manifestations. This is not just bookkeeping; at least some observations seem to be quite well fit by simple thermal modelling! We cannot hope to understand with any depth, or assess the need for, more complex calculations without a better understanding of our baseline modelling. Perhaps the simple solutions discussed here are revealing behaviour which will allow us to understand some of the interesting temporal features of a class of TDEs. The mathematical tools are now in place for studying evolving relativistic discs.

ACKNOWLEDGEMENTS

It is a pleasure to acknowledge useful conversations with K. Auchettl, R. Fender, J. Guillochon, K. Horne, P. Ivanov, W. Kley, J. Krolik, C. McKee, and E. Ramirez-Ruiz. Comments from our referee have improved the presentation. SAB acknowledges support from the Royal Society in the form of a Wolfson Research Merit Award, and from Science and Technology Facilities Council (STFC grant number ST/N000919/1).

REFERENCES

Abramowicz M. A., Czerny B., Lasota J. P., Szuszkiewicz E., 1988, ApJ, 332, 646
Abramowitz M. A., Stegun I. A., 1965, Handbook of Mathematical Functions. Dover, New York
Agol E., Krolik J. H., 2000, ApJ, 528, 161

Downloaded from https://academic.oup.com/mnras/article-abstract/481/3/3348/5094593 by Said Business School user on 14 November 2018

Auchettl K., Guillochon J., Ramirez-Ruiz E., 2017, ApJ, 838, 149 (AGR)
Balbus S. A., 2017, MNRAS, 471, 4832
Balbus S. A., Papaloizou J. C. B., 1999, ApJ, 521, 650
Cannizzo J. K., Lee H. M., Goodman J., 1990, ApJ, 351, 38
Eardley D. M., Lightman A. P., 1975, ApJ, 200, 187
Frank J., King A. R., Raine D. J., 2002, Accretion Power in Astrophysics. Cambridge University Press, Cambridge
Fromang S., Balbus S. A., Terquem C., 2002, MNRAS, 329, 18
Gradshteyn I. S., Ryzhik M., 2014, Table of Integrals, Series, and Products. Academic Press, New York
Hobson M. P., Efstathiou G., Lasenby A. N., 2006, General Relativity. An Introduction for Physicists. Cambridge University Press, Cambridge
Lynden-Bell D., Pringle J. E., 1974, MNRAS, 168, 603 (LBP)
Noble C. S., Krolik J. H., Hawley J. F., 2010, ApJ, 711, 959
Novikov I. D., Thorne K. S., 1973, in De Witt C., De Witt B., eds, Black Holes—Les Astres Occlus. Gordon and Breach, New York, p. 346
Paczyński B., 2000, preprint (arXiv:astro-ph/0004129)
Page D. N., Thorne K. S., 1974, ApJ, 191, 499
Penna R. F., McKinney J. C., Narayan R., Tchekhovsky A., Shafee R., McClintock J. E., 2010, MNRAS, 408, 752
Press W. H., Teukolsky S. A., Vetterling W. T., Flannery B. P., 2007, Numerical Recipes: The Art of Scientific Computing: 3rd ed. Cambridge University Press, New York
Pringle J. E., 1981, ARAA, 19, 137
Rees M. J., 1988, Nature, 333, 523
Riffert H., 2000, ApJ, 529, 119
Shafee R., McKinney J. C., Narayan R., Tchekovsky A., 2008, ApJ, 687, L25
Shakura N. I., Sunyaev R., 1973, A&A, 24, 337

APPENDIX: SOLUTION FOR KEPLERIAN POWER-LAW STRESS TENSOR

We present here the solution of equation (17) assuming that W^r_ϕ behaves as a power law in r throughout the Keplerian zone:

$$W^r_\phi = w_m (r/r_m)^\mu, \tag{A1}$$

where μ and w_m are constants. (We will assume that $W^r_\phi = w_m$ within the matching zone, remaining constant down to the ISCO.)

$$\frac{\partial y}{\partial t} = \frac{2 w_m r^\mu}{r_m^\mu \sqrt{GM}} \frac{\partial}{\partial r}\left(r^{1/2} \frac{\partial y}{\partial r}\right). \tag{A2}$$

With $\xi = r^{1/2}$ as in Section 2, this may be written as

$$\frac{\partial y}{\partial t} = \frac{w_m}{2 r_m^\mu \sqrt{GM}} \xi^{2\mu-1} \frac{\partial^2 y}{\partial \xi^2}. \tag{A3}$$

We seek the Laplace modes with time dependence e^{-st}. With y regarded as the Laplace amplitude, the equation becomes

$$\frac{\mathrm{d}^2 y}{\mathrm{d}\xi^2} = -\frac{2 s r_m^\mu \sqrt{GM}}{w_m} \xi^{1-2\mu}\ y \equiv -s\gamma^2 \xi^{1-2\mu} y, \tag{A4}$$

where

$$\gamma^2 = 2 r_m^\mu \sqrt{\frac{GM}{w_m^2}}. \tag{A5}$$

The solution to this equation is

$$y = r^{1/4} J_{\pm\frac{1}{4q}}\left(\frac{s^{1/2}\gamma r^q}{2q}\right), \quad q = \frac{3-2\mu}{4}. \tag{A6}$$

With $\xi = r^{1/2}$, we recover (21) in the limit $\mu \to 0$. If the inner boundary condition at $r = 0$ requires the vanishing of y, the positive index solution should be selected; otherwise both solutions are valid and should be retained throughout their region of validity.

The superposition of either one of these distinct solutions via a Laplace integral of the form (24) leads to the respective Green's function solutions:

$$y = \frac{r^{1/4}}{t} \exp\left[-\frac{\gamma^2 (r^{2q} + r_0^{2q})}{16 q^2 t}\right] I_{\pm\frac{1}{4q}}\left(\frac{\gamma^2 r^q r_0^q}{8 q^2 t}\right) \tag{A7}$$

for a ring initially laid down at $r = r_0$. This, in turn, leads to late-time luminosity behaviours of the form

$$L(\tau) \propto \tau^{-(1\pm 1/4q)}, \tag{A8}$$

where we have normalized the time via the dimensionless variable τ (Pringle 1981):

$$\tau = \frac{16 q^2 t}{\gamma^2}. \tag{A9}$$

Consider first $I_{\frac{1}{4q}}$, which is appropriate to a vanishing ISCO stress solution. This leads to

$$L(\tau) \propto \tau^{-(4-2\mu)/(3-2\mu)}. \tag{A10}$$

For declining outward stress, $\mu \leq 0$, this is always larger than unity – as found in our vanishing stress Newtonian calculations. Taking the $-1/4q$ solution leads, on the other hand, to

$$L(\tau) \propto \tau^{-(2-2\mu)/(3-2\mu)}, \tag{A11}$$

a power-law index always *less* than unity. This result is in better accord with observations. If we are indeed viewing the late stages of accreting discs in TDEs, it suggests a significant late-time admixture of solutions dominated by $J_{-1/4q}$ modes and a finite ISCO stress. This, in turn, is in good agreement with the $s \to 0$ analysis of Section 2.6.2.

A1: NUMERICAL METHOD

With Q defined by equation (4), the fundamental equation (2) may be written as

$$\frac{\partial \zeta}{\partial t} = \frac{e^Q W^r_\phi}{U^0} \frac{\partial}{\partial r} \frac{e^{-Q}}{U'_\phi} \left[\frac{\partial \zeta}{\partial r}\right]. \tag{A12}$$

Recall that we work in 'Boyer–Lindquist' coordinates in their near-equator form: t is time, as measured at infinity; r is cylindrical radius; ϕ is azimuthal angle, and z is height above equator. The line element is given by

$$\mathrm{d}s^2 = -\left(1 - \frac{2r_g}{r}\right)\mathrm{d}t^2 - \frac{4 r_g a}{r}\mathrm{d}t\mathrm{d}\phi + \frac{\mathrm{d}r^2}{1 - 2r_g/r + a^2/r^2} + \left(r^2 + a^2 + \frac{2 r_g a^2}{r}\right)\mathrm{d}\phi^2 + \mathrm{d}z^2. \tag{A13}$$

Downloaded from https://academic.oup.com/mnras/article-abstract/481/3/3348/5094593 by Said Business School user on 14 November 2018

The circular orbit solutions in the equatorial plane are given by (Hobson et al. 2006):

$$U_0 = -\frac{1 - 2r_g/r + a\sqrt{r_g/r^3}}{\left(1 - 3r_g/r + 2a\sqrt{r_g/r^3}\right)^{1/2}} \tag{A14}$$

$$U^0 = \frac{1 + a\sqrt{r_g/r^3}}{\left(1 - 3r_g/r + 2a\sqrt{r_g/r^3}\right)^{1/2}} \tag{A15}$$

$$U_\phi = \sqrt{r_g r}\,\frac{1 + a^2/r^2 - 2a\sqrt{r_g/r^3}}{\left(1 - 3r_g/r + 2a\sqrt{r_g/r^3}\right)^{1/2}} \tag{A16}$$

$$U^\phi = \frac{\sqrt{r_g/r^3}}{\left(1 - 3r_g/r + 2a\sqrt{r_g/r^3}\right)^{1/2}} \tag{A17}$$

$$\Omega = \frac{U^\phi}{U^t} = \frac{\sqrt{r_g/r^3}}{1 + a\sqrt{r_g/r^3}}. \tag{A18}$$

Using $\mathrm{d}Q/\mathrm{d}r \equiv -U_\phi U^\phi \mathrm{d}(\ln\Omega)/\mathrm{d}r$, direct calculation gives

$$e^{-Q} = \frac{1 + a\sqrt{r_g/r^3}}{\left(1 - 3r_g/r + 2a\sqrt{r_g/r^3}\right)^{1/2}} = U^0, \tag{A19}$$

and

$$U'_\phi = \frac{\sqrt{r_g}\left(a\sqrt{r_g} + r^{3/2}\right)\left(r^2 - 6r_g r - 3a^2 + 8a\sqrt{r_g r}\right)}{2r^4\left(1 - 3r_g/r + 2a\sqrt{r_g/r^3}\right)^{3/2}}. \tag{A20}$$

Substituting into the full evolution equation, we obtain

$$\frac{\partial\zeta}{\partial t} = \frac{2W^r_\phi}{\sqrt{r_g}(U^0)^2}\frac{\partial}{\partial r}\left[r^{3/2}F(r)\frac{\partial\zeta}{\partial r}\right], \tag{A21}$$

where

$$F(r) = \frac{1 - 3r_g/r + 2a\sqrt{r_g/r^3}}{r - 6r_g - 3a^2/r + 8a\sqrt{r_g/r}}. \tag{A22}$$

The position of the (apparently singular) ISCO is given by the solution of the equation $r_I^2 - 6r_g r_I - 3a^2 + 8a\sqrt{r_g r_I} = 0$. Numerical integration of the PDE is unstable in the vicinity of this point. This problem can be addressed by the substitution:

$$\rho = \left(r - 6r_g - \frac{3a^2}{r} + 8a\sqrt{\frac{r_g}{r}}\right)^2. \tag{A23}$$

There is no (simple) analytic expression for the explicit inverse $r = r(\rho)$, but numerically there is no difficulty with this inversion. Using

$$\frac{\partial\zeta}{\partial r} = 2\left(1 + \frac{3a^2}{r^2} - 4a\sqrt{\frac{r_g}{r^3}}\right)\left(r - 6r_g - \frac{3a^2}{r} + 8a\sqrt{\frac{r_g}{r}}\right)\frac{\partial\zeta}{\partial\rho} \tag{A24}$$

we may remove the numerical singularity at the ISCO. On full substitution of ρ for r, we have

$$\frac{\partial\zeta}{\partial t} = W^r_\phi A(\rho)\left[B(\rho)\frac{\partial\zeta}{\partial\rho} + C(\rho)\frac{\partial^2\zeta}{\partial\rho^2}\right] \tag{A25}$$

with

$$A = \frac{1 - 3r_g/r + 2a\sqrt{r_g/r^3}}{\sqrt{r_g}\left(1 + a\sqrt{r_g/r^3}\right)^2} \tag{A26}$$

$$B = \frac{6}{\sqrt{r}}\left(r - r_g - 8a\sqrt{\frac{r_g^3}{r^3}} - \frac{a^2}{r^2}\left(r - 17r_g\right) - 8a^3\sqrt{\frac{r_g}{r^5}}\right) \tag{A27}$$

$$C = 8r^{\frac{3}{2}}\left(1 - \frac{3r_g}{r} + 2a\sqrt{\frac{r_g}{r^3}}\right)\left(r - 6r_g - \frac{3a^2}{r} + 8a\sqrt{\frac{r_g}{r}}\right) \times \left(1 + \frac{3a^2}{r^2} - 4a\sqrt{\frac{r_g}{r^3}}\right)^2, \tag{A28}$$

where r is an implicit function of ρ. The numerical solution to this equation was found using the implicit finite difference method, with centred finite difference approximations used for spatial ρ derivatives and a forward difference approximation used for the time derivative (Press et al. 2007).

The derivation of the evolution equation is premised on small perturbations from circular orbits, and so within the ISCO it will quickly break down. Physically, we expect the fluid elements to quickly spiral into the Kerr hole after crossing the ISCO on a timescale similar to the free-fall time. This was demonstrated by Shafee et al. (2008), who found laminar flow in full GRMHD simulations within the ISCO. During this phase the fluid elements release almost no radiation and so barely contribute to the disc's spectra (Penna et al. 2010). Numerical integration of equation (65) is performed for the region of spacetime outside of the ISCO only ($\sqrt{\rho} > 0$), which is both mathematically self-consistent and physically sensible.

Once the full evolution equation has been solved, the time-dependent luminosity is straightforward to calculate. The local flux from a disc annulus is given by (Balbus 2017)

$$\mathcal{F} = -\Sigma U^0 W^r_\phi \Omega'. \tag{A29}$$

In full detail the luminoisty is rather complicated, but fortunately we are interested here only in the gross, late-time behaviour, not the precise spectral distribution. For this, a simple face-on disc model is more than sufficient, indeed the luminosity is largely from the Newtonian disc region. We retain the gravitational and kinematic redshift effects, which introduce the ratio of observed to emitted flux, $(U^0)^{-2}$, and neglect the photon orbit ('ray tracing') complications. The total observed luminosity is then given by

$$L(t) \propto \int_0^\infty \sqrt{g_{rr}g_{\phi\phi}}\,\frac{\mathcal{F}}{(U^0)^2}\mathrm{d}r. \tag{A30}$$

This may be written explicitly in terms of r as

$$L(t) \propto \int_{r_I}^\infty \frac{\zeta(r,t)\sqrt{r^2 + a^2(1 + 2r_g/r)}}{r^{7/2}\left(1 + a\sqrt{r_g/r^3}\right)^2\sqrt{1 - 2r_g/r + a^2/r^2}}\mathrm{d}r. \tag{A31}$$

We do not include the contribution of the disc with $r < r_I$ to the emitted luminosity, effectively terminating the disc emission at the ISCO. The integral (A31) was performed using a standard Simpson-type algorithm.

This paper has been typeset from a TEX/LATEX file prepared by the author.

Downloaded from https://academic.oup.com/mnras/article-abstract/481/3/3348/5094593 by Said Business School user on 14 November 2018